CHAPTER 5

Effect of USSP on Corrosion Resistance

5.1 INTRODUCTION

In this chapter, the effect of USSP on corrosion resistance of the as heat treated (900°C solution treated and water quenched) near-β Ti-13Nb-13Zr alloy in Ringer's solution, at room temperature is presented. The samples were subjected to 15 to 120 s of USSP treatment for corrosion study. The elemental composition of the alloy was assessed using energy-dispersive X-ray spectroscopy (EDS) in combination with SEM. The electrochemical study revealed reduction in corrosion of the USSP treated samples. There was maximum passivation in the specimen USSP treated for 30 seconds; however, it decreased with increase in the USSP duration. The improvement in the corrosion resistance from USSP was due to grain refinement and the associated compressive residual stresses in the surface region.

NOTE: In case of corrosion study, we have taken lower USSP duration up to only 120 seconds as further treatment duration will lead to rough surface. The high surface roughness will adversely affect the corrosion resistance.

5.2 USSP TREATMENT

Disc-shaped corrosion test samples of 12 mm diameter and 3 mm thickness were machined from the solution treated piece, mechanically polished on emery papers of 400, 800, 1000, and 1500 grit sizes on both sides, and finally mirror polished on rotating wheel mounting polishing cloth and using alumina powder (1μm) suspension in water.

Both sides of the disc-shaped samples were mechanically polished. The polished samples were cleaned in deionized water and subsequently in acetone using an ultrasonic cleaner. Both sides of the polished samples were then USSP treated alternately, with steel shots of 3 mm diameter by the ultrasonic horn (Stressonic Stress Voyager, France) vibrating at a constant frequency of 20 kHz and amplitude of 80 µm. The duration of USSP was varied from 15 to 120 s. The designations of the different samples are shown in Table 5.1.

Table 5.1 Designations of the USSP treated specimens.

USSP Treatment Duration (seconds)	**Designation**
15	USSP15
30	USSP30
60	USSP60
120	USSP120

5.3 CORROSION PROPERTIES

In order to analyze the effect of USSP treatment on corrosion resistance of the Ti-13Nb-13Zr alloy, electrochemical impedance spectroscopy (EIS) and potentiodynamic polarization tests were performed.

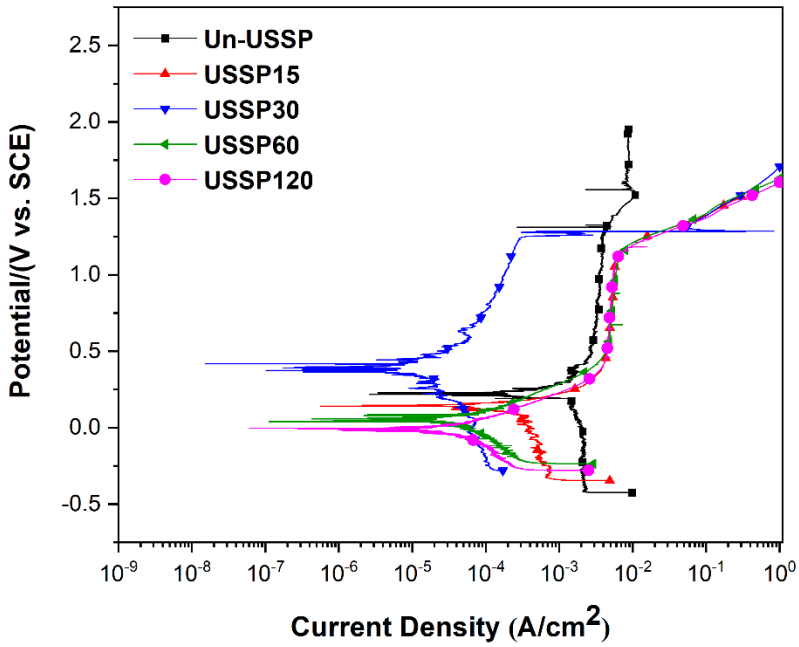

Figure 5.1 Potentiodynamic polarization curves of the Un-USSP and USSP treated samples.

Figure 5.1 illustrates the plots of the potentiodynamic polarization tests for the Un-USSP and USSP treated samples**.** The corrosion potential (E_{corr}), corrosion current densities (I_{corr}), and Tafel constants (β_a and β_c) were computed by Tafel extrapolation from cathodic and anodic branches of the polarization curves. For each sample, measurements were repeated thrice. The corrosion rate (CR) was calculated using the Faradays law [247] :

$$CR = I_{corr}\frac{K \times E_W}{D}\ (mm/yr) \qquad \text{(Equation 5.1)}$$

where K is the Faraday constant [3.272×10^{-3} mm g/μA cm yr], I_{corr} is corrosion current density (μA/cm^2), E_w is the equivalent weight (11.98 for Ti alloys) and D is density (5.01g/cm^3) of Ti -13Nb-13Zr [248]. Titanium is assumed to be major corroding species in the above calculations.

The values of the E_{corr}, I_{corr}, β_a, β_c, and corrosion rates are given in Table 5.2. A direct relationship can be observed between the E_{corr} values and corrosion resistance [249]. E_{corr} value is higher for the USSP30 sample compared to the other samples. Therefore, the USSP30 sample exhibits the highest corrosion resistance. The I_{corr} values are less for all the USSP treated samples in comparison with that of the Un-USSP sample. Evidently, the I_{corr} is much higher (1.135±0.05 μA/cm^2) for the Un-USSP sample, which exhibits a large active region**.** All the USSP samples exhibited passive breakdown at about 1.25 V. However, the Un-USSP sample exhibited steep passivity, even up to 2.5 V. While the USSP30 sample exhibited the lowest (0.09×10^{-3} mm/yr) corrosion rate, the Un-USSP sample exhibited the highest corrosion rate (8.87 ×10^{-3} mm/yr).

Table 5.2 Electrochemical parameters of the Un-USSP and USSP treated specimens extracted from polarization plots fitted in the Tafel regions.

Condition	**E_{CORR} (mV)**	**I_{CORR} (μA/cm^2)**	**βa (mV)**	**βc (mV)**	**Corrosion Rate (×10^{-3}, mm/year)**
Un-USSP	250.67	1.135	768.2	998.7	8.87
USSP15	142.295	0.159	101.1	259.6	1.24
USSP30	392.986	0.012	301.9	714.3	0.09
USSP60	42.361	0.052	189	337.3	0.40
USSP120	24.99	0.044	112.9	399	0.34

Further, from the electrochemical impedance spectroscopy (EIS), the Nyquist and Bode diagrams were established at respective OCPs for the Un-USSP and USSP treated specimens. In the Nyquist diagrams shown in Figure 5.2, the imaginary component of the impedance (Z_{img}) against the real part (Z_{real}) is obtained in the form of capacitive-

resistive semicircle for each sample. In order to predict the protection level of the oxide film and for the quantification of experimental EIS results, an equivalent circuit shown in Figure 5.3 is proposed based on the literature related to Ti alloys [250]. The experimental data are shown by the symbols and the simulated data are shown by the solid lines, which are generated by using the equivalent circuit. The experimental data were fitted well by EC-Lab (V11.27) software [251,252], using proposed equivalent circuit. The physical significance of all the circuit elements has been reported earlier in the literature [57]. With USSP treatment, an increase in the size of the capacitive loop (Figure 5.2) can be noted, indicating improvement in the corrosion resistance [254]. The impedance value for the Un-USSP treated sample is lower than that of the USSP treated samples, similar to the earlier observations [86,255]. This means that the USSP treated samples generates effective barrier layer and a passive film on the surface on immersion. Importantly, the area of the capacitive loop in the USSP30 is highest among the all which demonstrates nobler electrochemical behaviour.

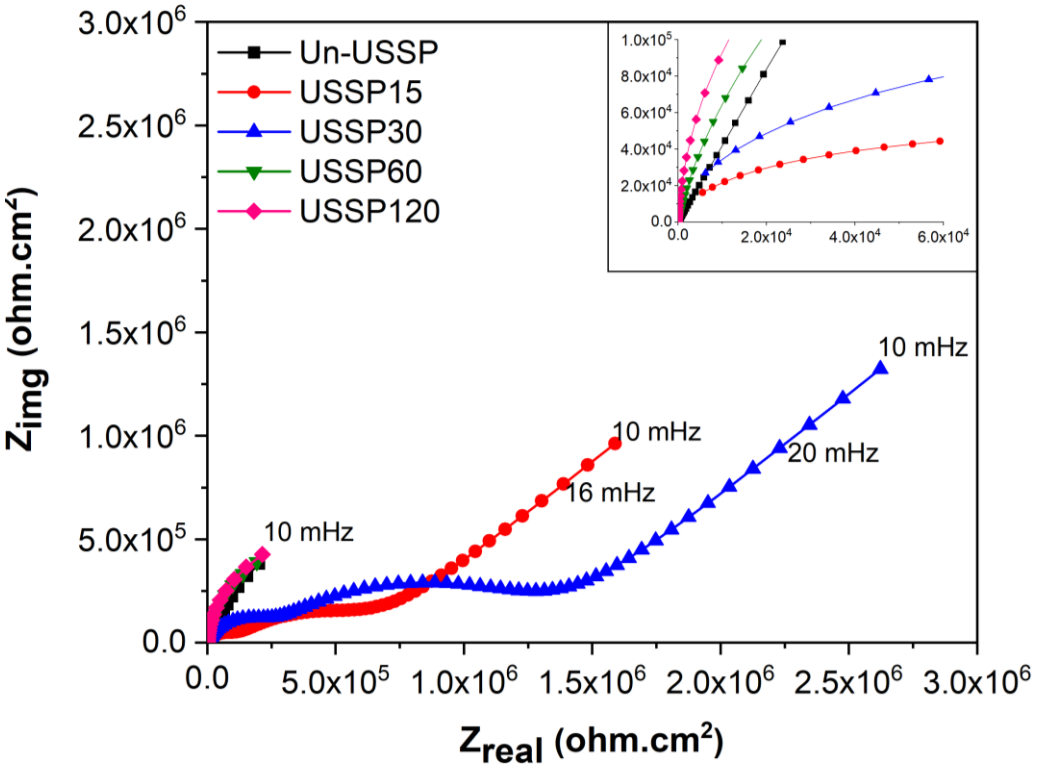

Figure 5.2 Nyquist diagrams of the Un-USSP and USSP treated Ti-13Nb-13Zr specimens.

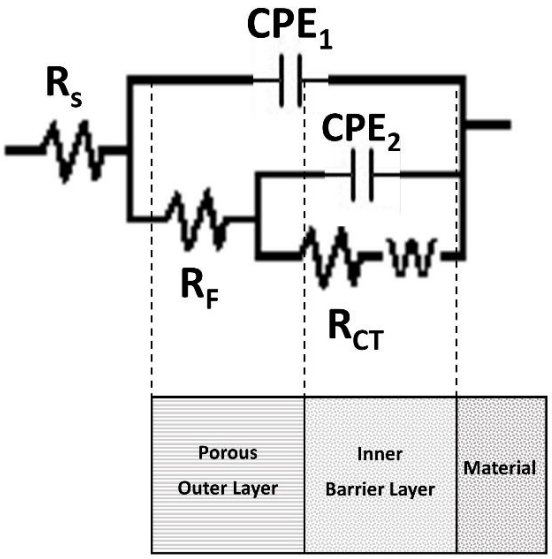

Figure 5.3 Equivalent circuit diagram for the fitting of EIS data.

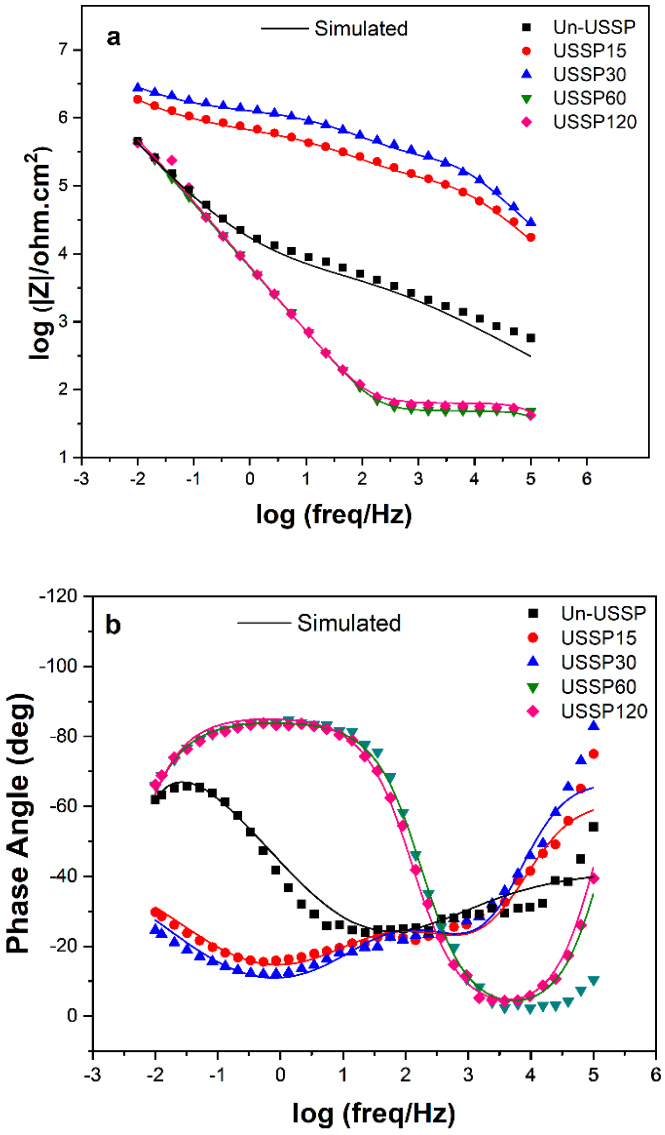

Figure 5.4 Bode diagrams (a)log-log plot of |Z| vs. freq. and (b)log-log plot of phase angle vs. freq., of Un-USSP and USSP treated specimens. The experimental data are shown by the symbols and the simulated data are shown as the solid lines.

Table 5.3 EIS data simulation for the Un-USSP and USSP treated specimens.

Specimens	R_S ($\Omega.cm^2$)	CPE_1 ($F.cm^{-2}\,sn^{-1}$)	n_1	R_F ($k\Omega.cm^2$)	CPE_2 ($F.cm^{-2}\,sn^{-1}$)	n_2	R_{CT} ($k\Omega.cm^2$)	W ($\Omega.cm^2$)
Un-USSP	31.87	$6.98x10^{-6}$	0.58	4.28	$42.9x10^{-6}$	0.97	867.13	21281
USSP15	33.60	$2.35x10^{-9}$	0.75	103.13	$0.18x10^{-6}$	0.51	888.80	258426
USSP30	36.22	$0.52x10^{-9}$	0.83	247.42	$5.77x10^{-8}$	0.56	1123.21	320708
USSP60	48.48	$26.1x10^{-6}$	0.95	475.11	$332x10^{-8}$	0.67	1051.12	27257
USSP120	54.06	$23.27x10^{-6}$	0.99	109.27	$13.6x10^{-8}$	0.96	1455.21	17252

High impedance values at low frequency indicate good corrosion resistance and low corrosion rate. It can be seen from Figure 5.4a that the impedance of the USSP15 and USSP30 sample are higher than that of the other samples. The phase angle vs. frequency curves in Figure 5.4b shows that the Un-USSP, USSP60, and USSP120 samples exhibit maxima, followed by a gradual decrease and again increase at the end. In contrast, the USSP15 and USSP30 samples showed increase in the phase angle for most of the frequency range.

Based on the electrochemical impedance spectroscopy, it was assumed that the oxide film formed on the Ti-alloys is composed of a porous outer layer and a barrier inner layer[99,100,256]. In this model, R_S, R_F and R_{CT} represent the resistance of solution, porous layer, and barrier layer, respectively. The constant phase elements (CPE) are chosen in the circuit for mathematical analysis of the impedance diagrams, where CPE_1 and CPE_2 represent capacitances of the outer porous and inner barrier layers, respectively. As diffusion plays an important role in the case of nanostructured materials, the Warburg component was also added in the equivalent circuit [257,258].

The impedance of CPE is shown by $Z_{CPE}=1/Q(j\omega)^n$, where ω is frequency, and n is CPE exponent. For pure resistance n=0 whereas for pure capacitance n=1. Q is CPE when the n value lies between 0.5 to 1. The value of each individual parameter is fitted and listed in Table 5.3. In the Ti-Al-Nb, Ti-Al-V, and Ti-Nb-Zr alloys, corrosion protection is due to the barrier layer [259]. Increase in the solution resistance can be observed with increase in the USSP duration. Comparison of the capacitance of the Un-USSP and USSP treated samples shows that the Un-USSP sample has higher capacitance (CPE_1 of about $6.98x10^{-6}$ $F.cm^{-2}$ sn^{-1}) and lower porous layer resistance (R_F=4.28 $k\Omega.cm^2$) than those of the USSP15 and USSP30 samples. This indicates that the Un-USSP sample has poor corrosion resistance, as also reported earlier [250]. The much

higher values of capacitance in the USSP60 and USSP120 samples indicate further decrement in corrosion resistance. The resistance of the barrier layer (R_{CT}) and outer porous layer (R_F) is higher for all the USSP treated samples compared to that of the Un-USSP samples. The R_F values are lower in acid and alkaline solutions than in the neutral solution, as consequence of the slightly higher corrosion; but the resistance of the barrier layer ($R_{CT),}$ remained high in acid and alkaline solutions, representing a resistant inner barrier layer, with high passivity [99]. The capacitances, CPE_1 and CPE_2 have decreased about 10^4 times and the inner barrier resistance (R_{CT}) has decreased by 10^2 times in case of the USSP30 treated sample compared to the Un-USSP sample. This reveals that the oxide film of the inner barrier layer in this specimen has increased significantly. A similar observation was also made by Cremasco et al. [250] in the Ti-35Nb alloy. When an electrochemical reaction is controlled by the absorption-penetration and diffusion, the impedance response exhibits a unique characteristic called the Warburg impedance. A sudden increase in the Warburg component was observed in the USSP15 and USSSP30 treated samples due to strong oxide layer formation, which is in line with the observation of Molavi et al. [260]. The deeper penetration of corrosion media creates Warburg resistance that leads to good capacitance and corrosion properties.

5.4 WEIGHT LOSS IN STATIC IMMERSION TESTS

The weight loss experiments for the samples immersed in Ringer's solution were performed for 35 weeks, and the data are plotted in Figure 5.5. All the samples showed continuous weight loss up to 14 weeks. The highest weight loss was in the Un-USSP sample, whereas it was the lowest in the USSP30 sample. After 22 weeks, a small weight gain can be observed in all the samples which could be due to the growth of the oxide layer. A similar trend in the weight gain was also observed by Karimi et al. [261] after 14 weeks in the alloy Ti-6Al-4V.

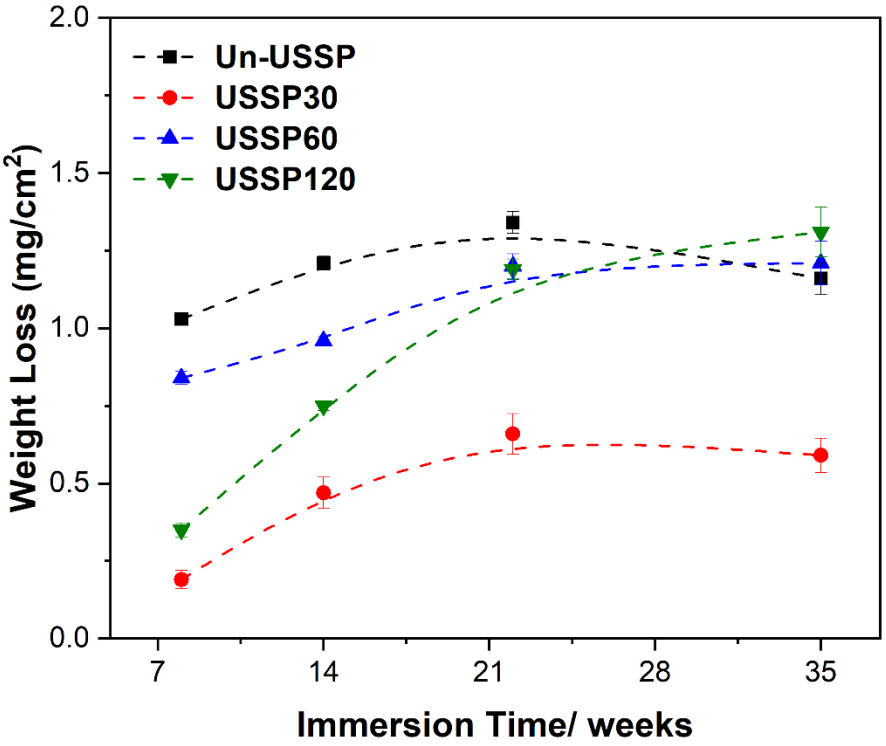

Figure 5.5 Weight change in the Un-USSP and USSP treated samples after static immersion in Ringer´s solution, at room temperature.

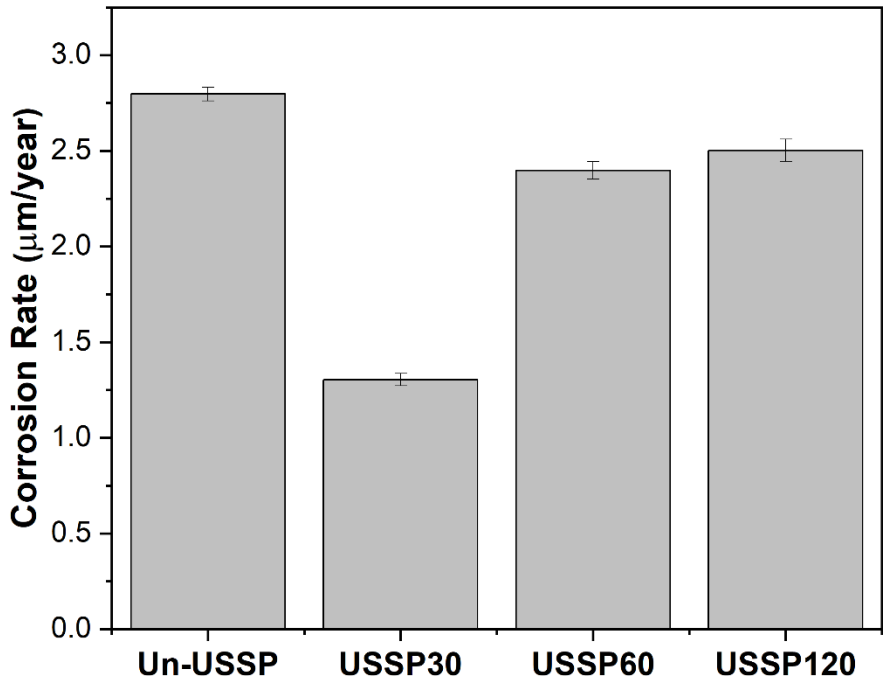

Figure 5.6 Corrosion rate of the Un-USSP and USSP treated samples after 35 weeks of immersion in Ringer's solution.

Weight loss data were used to calculate the corrosion rate of the samples in the Un-USSP and USSP treated conditions by the Equation 5.2 as per the ASTM G31-72.

$$Corrosion\ Rate(mm/year) = \frac{Q \times W}{A \times T \times D} \qquad \text{(Equation 5.2)}$$

where Q is a constant (87600), T is exposure time in hours, A is the area of immersed specimen in cm^2, W is the mass loss in mg and D is the density in gm/cm^3. The corrosion rates calculated from the potentiodynamic polarization tests were comparable with the corrosion rates calculated from intermittent exposure of the Un-USSP and USSP treated samples in Ringer´s solution for 35 weeks, and the results are shown in Figure 5.6. The weight loss of the samples follows the order as USSP30<USSP60<USSP120<Un-USSP. The USSP treated samples showed a relatively slower rate of corrosion and less weight gain. Figure 5.7(a-h) shows the secondary electron SEM images along with the EDS of all the samples after 35 weeks of immersion in the Ringer's solution. The USSP60 and USSP120 samples in Figure 5.7e and g show serious localized corrosion and globular corrosion products were visible on the surface of the samples. However, the USSP30 (Figure 5.7c) sample showed a clear surface without any localized corrosion deposits. The Un-USSP (Figure 5.7a) sample also showed small micron size corrosion products deposited on the surface.

The weight percentages (wt.%) of the elements detected by EDS analysis shown in Figure 5.7b, d, f and h were primarily of Ti, Zr, Nb and O. The presence of oxygen in all the species indicates that the surface was covered with an oxide layer.

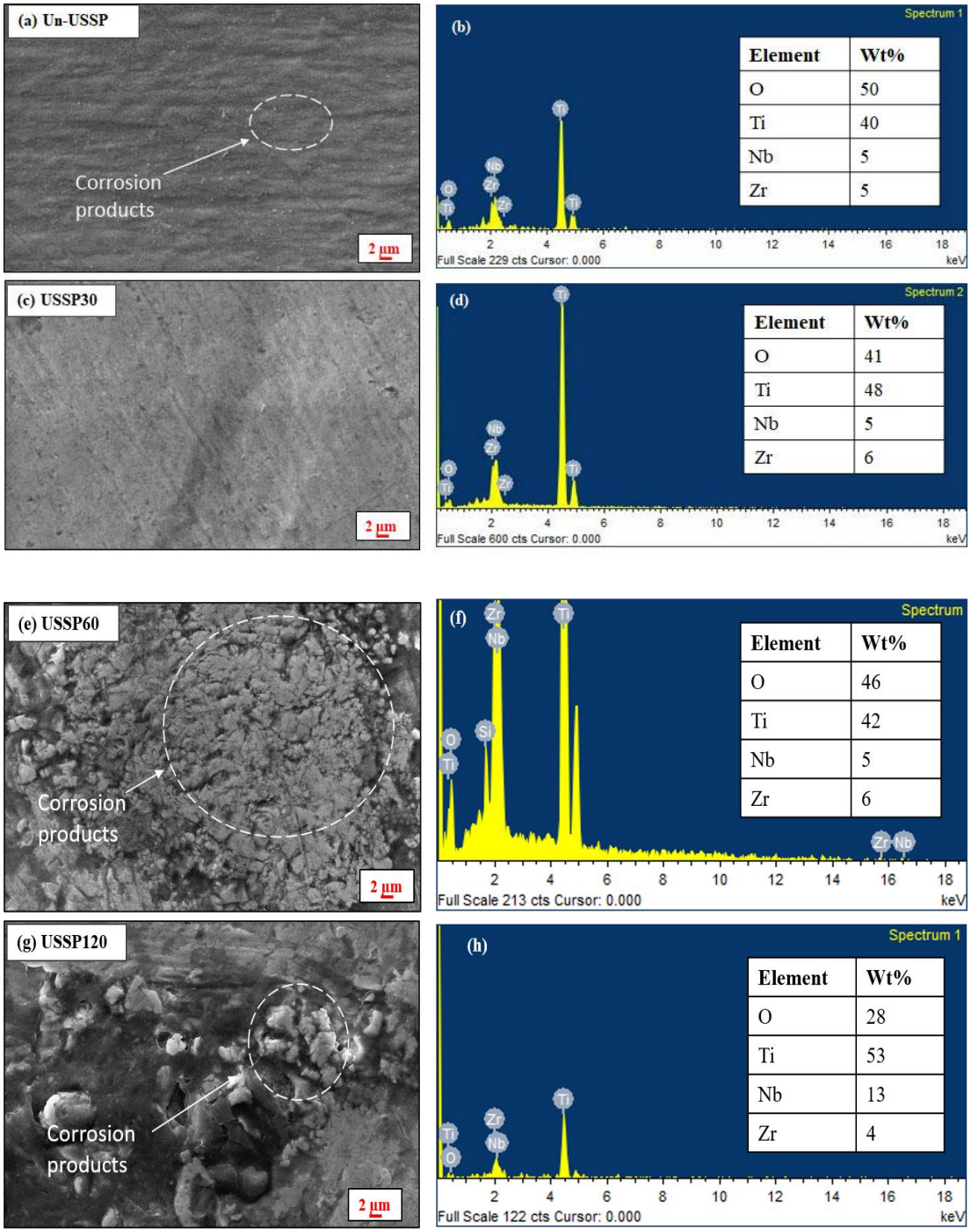

Figure 5.7 SEM (secondary electron) images along with EDS of the (a) Un-USSP, (c) USSP30, (e) USSP60, and (g) USSP120 samples after 35 weeks of immersion in the Ringer´s solution.

Oxides such as TiO_2, Nb_2O_5, and ZrO_2 thus formed on the surface of the Ti-13Nb-13Zr alloy. The higher wt% of Ti in the USSP30 sample compared to that on the Un-USSP sample indicates stable and thick oxide layer formation on the USSP30 sample.

5.5 CHEMICAL ANALYSIS BY XPS

XPS characterization of the Un-USSP and USSP30 treated samples was performed after 48 h of immersion in the Ringer´s solution. These samples were removed from the corrosive media and rinsed with water and ethanol, and then dried. Figure 5.8 and Figure 5.9 display XPS survey and high-resolution XPS spectra for both the Un-USSP and USSP30 treated specimens showing the presence of Ti, C, O, Nb, Zr, and Na elements. In the XPS data, the Ti 2p spectra of the passive layer show a double peak of Ti $2p^{3/2}$ at 458.5 eV, and Ti $2p^{1/2}$ at 464.3 eV, which are binding energies of the TiO_2. The two Nb 3d peaks at 207.6 eV, and 210.4 eV confirmed the presence of Nb_2O_5 oxide.

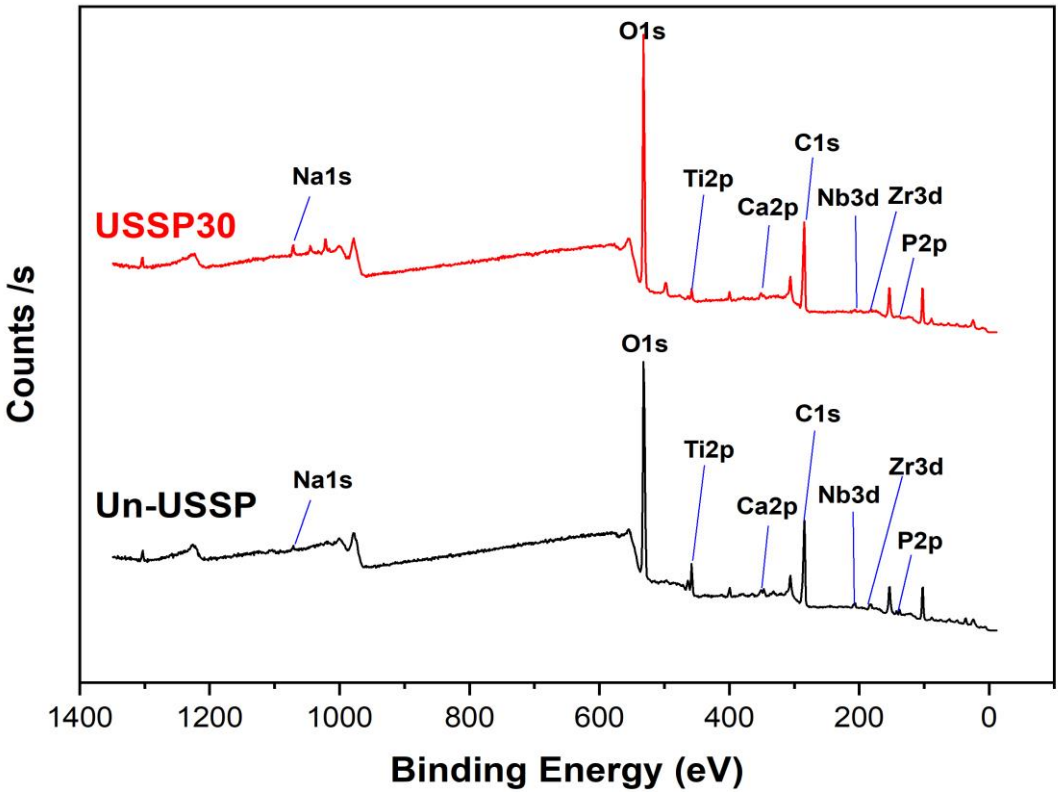

Figure 5.8 Typical XPS survey data of the USSP30 and Un-USSP specimens.

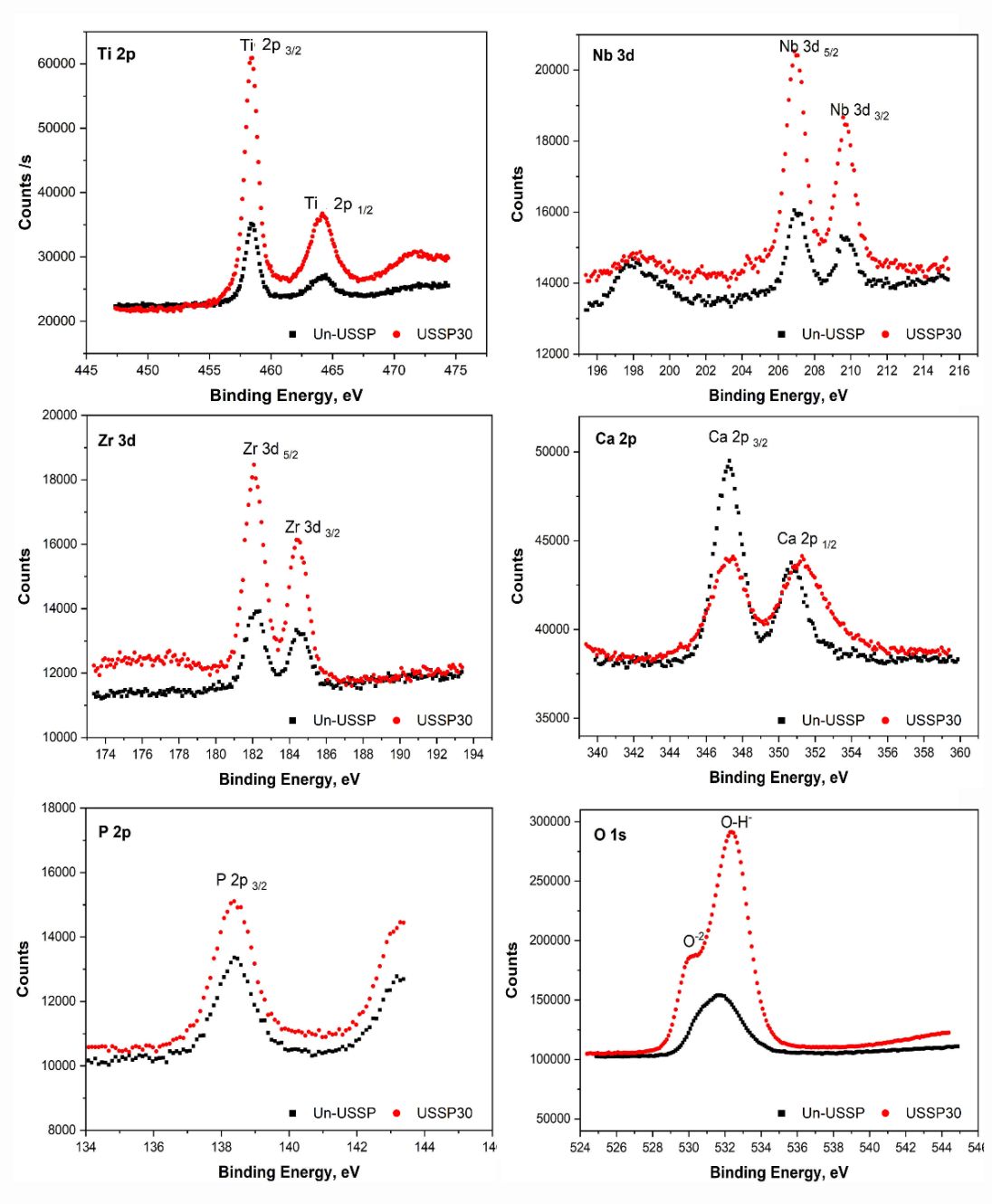

Figure 5.9 High resolution XPS showing Ti 2p, Nb 3d, Zr 3d, Ca 2p, P 2p, and O 1s of the Ti-13Nb-13Zr alloy, in the Un-USSP and USSP30 condition.

Table 5.4 Surface composition from XPS spectra of Un-USSP and USSP30 sample.

Sample	Concentration, atomic%								
	O	**C**	**Si**	**Na**	**Ti**	**Zr**	**Nb**	**Ca**	**P**
Un-USSP	22	21	7	0.19	1.4	0.15	0.14	0.64	0.15
USSP30	40	42	13	1.04	1.2	0.10	0.11	0.74	0.04

The two peaks of Zr 3d at 183 eV and 185.2 eV, could be from ZrO_2. The spectra of P 2p and Ca 2p with peak binding energy of 138.87 eV and 348.04 eV indicates the presence of a calcium phosphate compound on the alloy surface. The spectrum of O 1s at 532.09 eV indicates oxide on the surface of the sample, in line with the earlier observation [262]. In Figure 5.9**,** the observed spectra intensities were higher for the USSP30 than those of the Un-USSP condition, which can be explained by the formation of more TiO_2, Nb_2O_5, and ZrO_2 native film on the USSP treated alloy surface [179]. Also, the data given in Table 5.4 show a noticeable enrichment of oxygen on the USSP30 samples, indicating that USSP treatment increases the formation of the passive oxide layer.

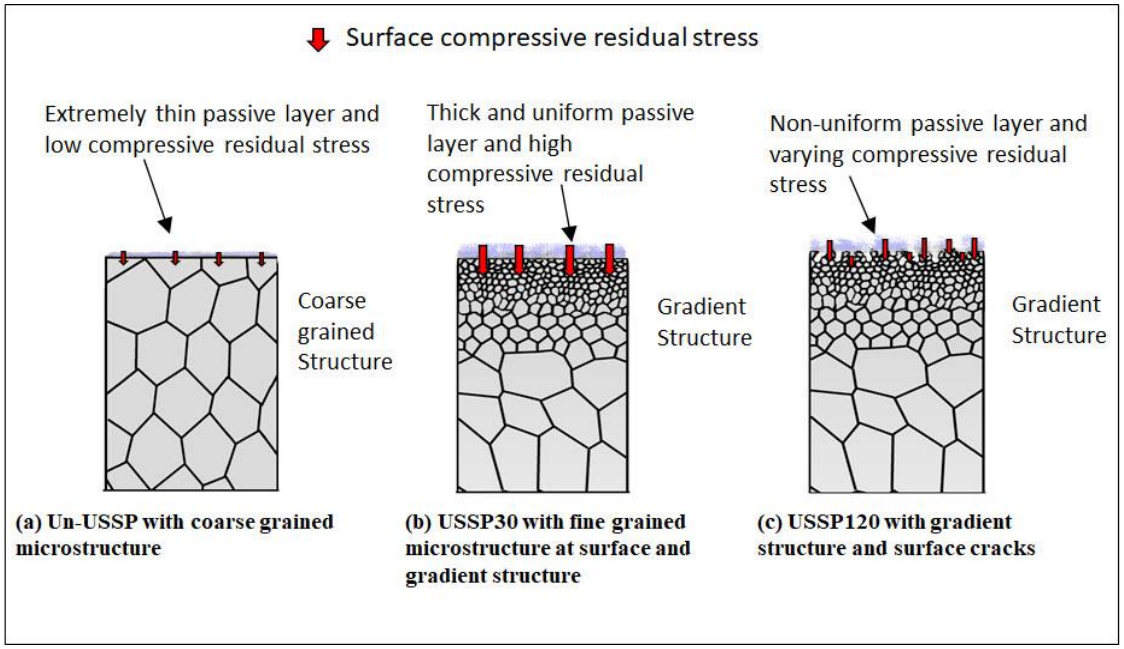

Figure 5.10 Schematic illustration of the passive layer and associated compressive residual stress in different conditions (a) Un-USSP, (b) USSP30, and (c) USSP120 samples.

5.6 DISCUSSION

5.6.1 Microstructure

In the Un-USSP condition (Figure 5.10a), there is coarse grained microstructure of micron size, formation of very thin and non-uniform passive layer associated with very small compressive residual stress on the surface. In the USSP30 condition (Figure 5.10b), it may be seen that there is formation of uniform and compact passive layer of appreciable thickness, associated with high residual stress, in the nano structured surface region. Also, there is formation of gradient microstructure. The magnitude of associated compressive residual stress is highest at the surface and decreases with increase in depth from the shotpeened surface. In the USSP120 condition (Figure 5.10c) microstructure in the surface region is similar to that of the USSP30; however, there is localised cracking and the surface layer is nonuniform with varying residual stress. The residual stress is relieved in the cracked region. In the present investigation, the residual stresses are correlated with the microstructural changes occurring from the process of severe plastic deformation. Roland et al. [246] partially ascribed the near-surface residual stresses to high dislocation density inside the material.

5.6.2 Effect of USSP on Corrosion Behaviour

Titanium alloys are important for biomedical applications as they quickly develop a passive oxide layer on their surface, which can be either crystalline, amorphous, or Un-stoichiometric. Potentiodynamic polarization experiments are used to determine the corrosion performance of alloys in the various environments as well as to assess their corrosion rate. The values of E_{corr}, I_{corr}, and corrosion rates in Table 5.2 show that E_{corr} is the highest and the I_{corr} is lowest for the USSP30 among all the samples, including the Un-USSP. Corrosion resistance is affected by the synergistic effect of grain refinement, surface roughness and compressive stresses on the surface. The grain refinement and

compressive residual stress help in improving the corrosion resistance [113,263]; whereas, the surface roughness decreases the corrosion resistance. With grain refinement, the corrosion rate is decreased, and E_{corr} shifts towards the noble direction [251], as emphasized later in this section. However, with increase in the roughness, the active surface area increases; therefore, the corrosion rate also increases [264]. The sudden increase in roughness of the USSP15 specimen compared to that of the Un-USSP (Table 4.3) decreased the E_{corr} value, however, the corrosion resistance was higher. The magnitude of positive effect, resulting from the grain refinement and induced compressive residual stress in USSP15 sample was reduced due to negative effect of increased surface roughness, on the corrosion resistance. In the USSP30 sample compared to USSP15, there was only nominal decrease in the grain size in respect of that of the USSP15 but increase in the compressive residual stress was nearly 100% and the surface roughness was increased only by 24%. Therefore, the positive effect of the residual compressive stress induced in the USSP30 was significantly higher than that in the USSP15 and corrosion resistance of the USSP30 was significantly enhanced. However, the longer durations of the USSP treatment of 60 and 120 s increased the roughness and cracking tendency at the surface, as evident from SEM images in Figure 4.7. The overall positive effect of grain refinement and compressive residual stress on the corrosion resistance was neutralized due to relieving of the compressive residual stresses (Figure 4.10) and due to the excessive damage of the surface of the USSP60 and USSP120 samples. Therefore, the E_{corr} values shifted towards the active side in the USSP60 and USSP120 samples. The severity of corrosion therefore, follows the order as USSP30<USSP120<USSP60<USSP15<Un-USSP. Despite the low current density of the USSP treated samples, the growth of passive oxide layer was facilitated by the active sites in the surface of the alloy.

It is evident from Figure 4.7 that the degree of inhomogeneity increases from the USSP30 to USSP120, and sharp edges, cracks and chipping were clearly visible in the USSP treated samples. The inhomogeneity on the surface resulting from the USSP treatment provides an easy diffusion path for the transfer of ions [265]. However, with increased plastic deformation, the formation of an effective passive layer is delayed and localized corrosion is enhanced.

The above results imply that the corrosion behaviour of the Ti-13Nb-13Zr alloy is greatly affected by the surface modification caused by the USSP treatment, and it is essential to discuss the reasons that resulted in the formation of stable oxide film on the surface of the USSP30 sample compared to that on the Un-USSP sample. Grain refinement in the surface region can be observed from the XRD (Figure 4.3) and TEM images **(**Figure 4.5b-d). The reduction in grain size played an important role in enhancing electronic activity at grain boundaries [266]. The increased electronic activity decreases the work function, and the surface becomes more electrochemically active towards passivation. Huang and Han studied corrosion behaviour of the SMAT treated Ti–25Nb–3Mo–3Zr–2Sn alloy and found considerable increase in corrosion resistance when the surface grain size was decreased from micro to nanoscale [237]. They correlated it with the dilution of the segregated elements at grain boundaries which results in the formation of a stable and thicker passive oxide layer on the surface nanograined specimens. The USSP treated samples oxidized much rapidly because of the higher density of grain boundaries and increased surface energy [210]. The enhanced corrosion resistance of the USSP treated samples can be ascribed to rapid formation of a protective oxide layer on the top surface, which also improves the chemical stability of the alloy by decreasing the diffusion of ions and the activity of charge carriers at the interface between electrolyte and substrate [88]. The abundance of grain boundaries in the nanocrystalline layer also

improves the interfacial bonding of the passive layer [263]. It has been reported that 15 s and 90 s of USSP treatment in Al 7075 and CP-titanium improved the corrosion resistance, which on further treatment decreased due to an increase in the density of defects and the surface inhomogeneity [187,267].

The surface roughness was found to increase with the USSP duration. Earlier studies have shown that with increased surface roughness, the effective area of corrosion increases and corrosion resistance deteriorates [268]. Therefore, with an increase in the USSP duration from 30 to 120 s, increase in the roughness caused loss in corrosion resistance. The presence of cracks, plate type structures, and separated regions (Figure 4.7c-d) have also deteriorated corrosion resistance of materials as they constitute a local potential difference in terms of electrochemical behaviour.

Balakrishnan et al. [263] studied the corrosion behaviour of ultrafine-grained Cp-titanium. They speculated presence of high residual stresses at the surface from shifts in the XRD peaks, which can also improve corrosion resistance. The reduction in corrosion current density following the USSP treatment (see Table 5.2) can be associated with the increased compressive residual stresses in the USSP treated samples (Figure 4.10), which help in formation and growth of a compact passive oxide layer. Similar results were also reported in aluminium alloys in which the developed compressive stresses suppressed rupture of the passive layer in contrast to tensile stress [269]. The process of passive layer formation can be different for different alloys but the role of the compressive stresses can be considered identical, being preventive for the passive layer. Also, in AISI 316L stainless steel [270], the presence of compressive residual stresses decreases the interatomic distances, thereby making thicker layer of chromium atoms near the surface that assist in the formation, growth and strength of the passive layer. The effect of residual stresses on localized corrosion of different metals has also been reported in the

literature [269,271]. According to Ghosh et al. [272], the austenitic stainless steels having tensile residual stresses at the machined surface are highly susceptible to chloride attack.

The process of USSP can also increase oxygen levels at the subsurface compared with the untreated condition. Thomas et al. [273] have reported increased oxygen in the sub-surface of SMAT treated near-α titanium alloy compared to the untreated, which can be ascribed to the faster diffusion along the twin boundaries and dislocation slip bands within the plastically deformed surface layer. The process of surface grain refinement also provides a high density of nucleation sites for the formation of a dense passive layer and thereby decreases corrosion rate [274]. The water content inside the solution supplies oxygen (O^{2-}) ions which help in development of TiO_2. Due to the applied current, an electrostatic field is set up across the oxide that maintains Ti oxidation and movement of O^{2-} ions inward and Ti^{4+} ions outward and thus leads to a continuous growth of the oxide layer. The anode reaction can be shown according to the Equation 5.3 [275]:

$$Ti + 2H_2O \rightarrow TiO_2 + 4H^+ + 4e^- \quad \text{(Equation 5.3)}$$

Also, the electrolyte contains Cl^- ions, and there is adsorption of chloride ions on the titanium alloy surface, which forms a chemisorbed complex which on further hydrolysis again forms titanium oxide according to the following equations (Equation 5.4 and Equation 5.5) [275]:

$$Ti+4Cl\text{-}\rightarrow[TiCl_4]^-\rightarrow TiCl_4+4e^- \quad \text{(Equation 5.4)}$$

$$TiCl_4+ 2H_2O \rightarrow TiO_2+4Cl^-+ 4H^+ \quad \text{(Equation 5.5)}$$

Warburg component in low-frequency region corresponds to the effect of concentration polarization, dominated by diffusion on the electrode reaction [276]. Warburg-type diffusion component in the EIS spectrum can be ascribed to diffusion processes occurring in the solid phase. According to Munirathinam et al. [277] Warburg component is mainly

due to diffusion of titanium ions to porous layer. Narayan et al. [278] also described that upon immersion in bio-fluids the Warburg component first decreases and then attains a constant value. This suggests that the micro/nano pores in the outer part of the passive film act as diffusion sites for ions and molecules present inside the solution [279].

The values of phase angles shown in Figure 5.4b in the high-frequency region reflect that the tested samples have rough and convoluted surface [280]. The absolute value in all the samples is less than 90° due to the non-uniformity of the electrochemical system and of the alloy [281]. As the phase angle increases, the possibility of corrosion decreases.

In Figure 5.5 the USSP30 and USSP60 samples show lower weight loss compared to the Un-USSP sample due to surface grain refinement. Beddoes et al. [282] have shown the effect of surface roughness on the weight loss of the 316L stainless steel during 72 hours of immersion in ferric chloride solution and reported faster weight loss at higher roughness at 22°C. There are reports in the literature that have shown that rougher is the surface more will be the ions released [48,283]. The large size cracks and discontinuities shown in Figure 4.7c and d on the surface of the USSP60 and USSP120 samples promoted localized corrosion and greater weight loss compared to the USSP30 sample.

Liu et al. [284] demonstrated that improvement in corrosion resistance of the Ti-10V-2Fe-3Al alloy due to formation of stable and thick oxide film by sealing of micro and nanopores. After immersion in the Ringer´s solution, the outer porous layer will be filled with water molecules and precipitated compounds; hence the pores get self-healed that also contribute to the high impedance values [285]. The ions from the solution go through the narrow channel formed by the surface micropores and micro-cracks so that the reaction takes place from outside to inside. Since the roughness of the USSP30

sample is less and also micropores are visible on the surface after USSP treatment (**see** Figure 4.7b), the sealing effect due to the formation of the precipitated compounds like calcium phosphate [286] and deposits of TiO_2 into the micropores enhances the passivity behaviour of the USSP treated samples, as clearly seen from the Nyquist plot and lesser weight loss.

The weight gain after 22 weeks in case of all the samples (Figure 5.6) could be due to the dissolution of titanium ions and formation of titanium oxide on the surface [287]. In static immersion tests it is believed that more titanium ions will be released into the solution if the exposure time is more. However, in a study by Karimi et al. [261] on Ti-6Al-4V alloy showed that the release of Ti ion was reduced after 14 weeks due to precipitation of dissolved ions. Huang et al. [48] investigated the release of Ni-Ti ions in artificial saliva. In their study, the amount of Ti release increased up to 14 days and then stopped with further increase in the immersion durations. The USSP60 and USSP120 samples showed serious localized corrosion, and corrosion products were observed at scattered locations. This type of corrosion is also known as pitting-type localized corrosion. From the SEM images (Figure 5.7e and g) after 35 weeks of immersion in Ringer´s solution, it may be observed that the corrosion mainly started at the large defects and cracks that were formed on the surface of the samples after the USSP treatment. Luqman et al. [13] also observed similar type of corrosion on the surface of the Ti-6Al-4V alloy. It is clear from the Figure 5.7c of the USSP30 sample that the surface of this specimen is covered with a compact oxide film, and there is no visible corrosion. Jin et al. [88] studied corrosion behaviour of the SMAT treated Ti-Nb-Zr-Fe alloy and also observed a dense and compact oxide layer on the nanocrystalline surface. The micron-sized corrosion products seen in in Un-USSP samples (Figure 5.7a) indicate weak corrosion resistance. The increased surface defects in the USSP60 and USSP120

samples decreased the stability of the passive film. The XPS spectra analysis showed noticeable enrichment of oxygen after the USSP treatment (Figure 5.8), suggesting formation of more protective passive layer (TiO_2, ZrO_2, and Nb_2O_5) on the surface of the USSP treated samples that enhanced the protection of the studied alloy against further corrosion.

XRD analysis of the USSP treated samples revealed that surface grains were refined up to 21 nm. This refinement of surface grains from micro to nano level enhanced the formation of the passive layer. Polarization test, EIS studies, and the long-term immersion tests have validated that the USSP30 sample shows the best corrosion resistance due to much higher effectiveness of the passivation as it shows nano crystallized surface with least defects. The USSP60 and USSP120 samples show further refinement in the surface microstructure, but the effect of passivation on corrosion resistance decreases due to an increase in the unevenness of the surface, increase in the density of defects, and the tendency for surface cracking. Hence, it is obvious that the phenomenon of grain refinement in the near-surface region is not the only factor for governing corrosion resistance of metals. In the USSP30 samples, the positive effect of reduction in the crystallite size along with optimum compressive residual stress and surface roughness improved corrosion resistance of the Ti-13Nb-13Zr alloy compared to the Un-USSP samples. It is important to point out that there is an increase in the corrosion resistance of all the USSP treated samples. It may be concluded that by optimising the stress state, grain size, and roughness at the surface of the alloy, the corrosion resistance can be improved significantly.

5.7 CONCLUSIONS

Initially, a low modulus Ti-13Nb-13Zr alloy was USSP treated for different durations of 30 to 120 s, that resulted in successful development of nanograins and high compressive residual stress in the surface region. Then the electrochemical study was done to highlight the effect of USSP treatment on the corrosion resistance of the alloy. Following conclusions are drawn from this chapter:

1. It is important to point out that there is an increase in the corrosion resistance of all the USSP treated samples. However, decrease in passivation was observed after 30 s of USSP treatment, which can be mainly attributed to increased surface roughness and cracking tendency caused by the excessive plastic deformation. The best corrosion resistance was observed after 30 s of USSP treatment.
2. XPS study of USSP30 treated samples showed the presence of higher protective oxides (TiO_2, ZrO_2, and Nb_2O_5) formed on the surface compared to Un-USSP condition.
3. Electrochemical corrosion and static immersion tests both have validated that 30 s of USSP duration has improved the corrosion resistance significantly by forming an intact passive oxide layer and provided good corrosion resistance to the inner substrate layer.
4. The grain refinement and surface roughness were the two opposing factors controlling the corrosion behaviour. Besides grain refinement, the presence of compressive residual stresses with appropriate USSP duration produced optimal corrosion resistance.
5. It may be concluded that by optimizing the compressive residual stress, grain size, and roughness at the surface of the alloy, the corrosion resistance can be improved significantly.